

Load–settlement response of shallow foundations resting on granular soil

Mohamed Nimeri¹ · Sherif Elfass¹ · Gary Norris¹

Received: 3 May 2017 / Accepted: 2 June 2017 / Published online: 26 June 2017
© Springer International Publishing AG 2017

Abstract Proper estimation of settlement of shallow foundations resting on granular soil deposits has a significant role in the design and construction of buildings and other related structures. While several procedures are available in the literature, discrepancies still exist between the predicted and observed responses. Furthermore, there is a decoupling between bearing capacity and settlement assessment for the same foundation and soil type. This paper presents a new model which was developed to assess load–settlement response up to ultimate soil failure. The model utilizes Mohr–Coulomb criteria coupled with a stress–strain relationship that captures the behavior of granular soil up to large strains. The model has been verified using documented results reported in the literature. Furthermore, two full-scale plate load experiments were recently performed at the University of Nevada, Reno (UNR), utilizing a large soil box 10 ft. (3.048 m) × 10 ft. (3.048 m) × 7 ft. (2.134 m). The experiments modeled single-layer and multi-layer soil structure. The load–settlement responses up to bearing capacity failure are reported for both experiments.

Keywords Shallow foundation · Bearing capacity · Settlement

This paper was selected from GeoMEast 2017—Sustainable Civil Infrastructures: Innovative Infrastructure Geotechnology.

✉ Gary Norris
norris@unr.edu

Mohamed Nimeri
mnimeri@nevada.unr.edu

Sherif Elfass
elfass@unr.edu

¹ Department of Civil and Environmental Engineering,
University of Nevada, Reno, Reno, NV 89557, USA

Introduction

Foundations are essential for engineered structures, transmitting and distributing the supported loads into the underlying soil structure. Engineers typically aim for designs where soil pressures at all depths are maintained within acceptable levels, preventing soil shear failure and limiting soil settlements within tolerable levels. Foundation settlement starts as early as during construction, and increases gradually as the load is increased. This load–settlement response, if permitted, continues up to the point where the load per unit area equals ultimate pressure, at which the soil supporting the foundation fails, referred to as the ultimate bearing capacity (q_{ult}).

The classical solution for Ultimate Bearing Capacity of soil with cohesion, c , and friction angle, ϕ , is typically assessed based on a bearing capacity equation composed of three terms, as a function of the pressure generated by the foundation width, B , embedment depth, D_f , and c ; as in Terzaghi, Meyerhof, Hansen and Vesic models. Each term is multiplied by a bearing capacity factor; these factors are a function of ϕ . These models are thoroughly reported in the literature. For instance, The Army Corps of Engineers (republished by ASCE [1]) provides a comprehensive listing of Terzaghi, Meyerhof, Hansen, and Vesic equations and factors. While there is an agreement on the basic bearing capacity equation, differences regarding the form of the factors exist between them.

However, the equations for bearing capacity factors are largely theoretical utilizing multiple correction factors that are semi-empirical in nature, based on lab scale model tests, where B is usually less than 12 inches. Only a few field tests with more realistic values of B have been documented in the literature. Then again, most field

tests are usually terminated as some arbitrarily predetermined failure criterion based on settlement, rather than carrying out the test to the ultimate soil failure where no additional load carrying capacity is observed, regardless of the settlement. Hence, these solutions provide an ultimate bearing capacity value without regard to the progression of the load response (up to failure), then this load response is decoupled from the corresponding settlement response.

It is time to re-examine bearing capacity on a fundamental but practical basis, without some of the complexities (inclined load, inclined base, eccentricity, foundation shape, and choice of strength test) to better judge what occurs and how to calculate it realistically. The goal is to address the stress–strain–strength behavior of the soil and its variation with pressure, to capture the load–settlement response culminating in true bearing capacity failure and to compare it with well-documented field and large-scale lab tests that are supported with adequate soil data.

The model is based on standard triaxial test stress–strain–strength behavior, since large-scale lab or field test information from the literature will in most cases be for square or circular foundations. The model provides a full load–settlement curve, up to ultimate bearing capacity, giving a detailed picture of the soil behavior during the mobilized state progressing to failure. Eventually, engineers will apply their desired failure criteria (e.g., 0.5 inch settlement), knowing the expected progression of load–settlement response, up to the ultimate bearing capacity failure. In fact, the resulting predicted curve should be directly comparable to the field load–settlement curve, up to and sometimes beyond the field test failure criterion.

Proposed model

The failure mechanism under shallow foundations can be separated into three zones (or wedges), as shown in Fig. 1. The interdependent stress state of the three zones, and Mohr–Coulomb failure envelope are illustrated in Fig. 2. The minor principal stress of zone I is the effective overburden pressure, P_o , at the depth of $0.5 B j$ where j is taken as $1.5 \tan \phi$ (after Hansen). The vertical or major principal stress of zone III at the same depth is $(q_{ult} + 0.5 B j \gamma_y)$. Zone II of Fig. 1 (represented by a dashed Mohr circle II of Fig. 2) is the classical radial shear zone over which stress state is continuously varying from that of the boundary of zone I to that of zone III. Note that γ_x and γ_y are the effective unit weights of the respective soil above and below the foundation base at embedment depth D_f below soil surface. Effective horizontal pressure, P_h , the major principal stress of zone I, is also the minor principal stress of zone II. Likewise, the major principal stress of the dashed Mohr circle of zone II is the minor principal stress of zone III.

A new origin, O' , at the distance $(c/\tan \phi)$ from O is introduced to deal with just a frictional material, ϕ . Based on the new origin, the c – ϕ envelope relative to O becomes a ϕ envelope relative to the transformed origin O' . Hence, the effective overburden pressure of zone I relative to O' is

$$P_{o*} = P_o + c/\tan \phi$$

$$P_{o*} = D_f \gamma_x + 0.5 B j \gamma_y + c/\tan \phi; (j = 1.5 \tan \phi)$$

Note that the horizontal distance between the lower end or minor principal stress of circle I and the upper end or major principal stress of circle III is the net ultimate bearing pressure, q_{net} , while q_{ult} is the ultimate bearing capacity or the gross pressure applied at the base of the foundation at failure, as shown in Fig. 2. The net pressure

Fig. 1 Three zone model of developing failure mass in shallow foundations

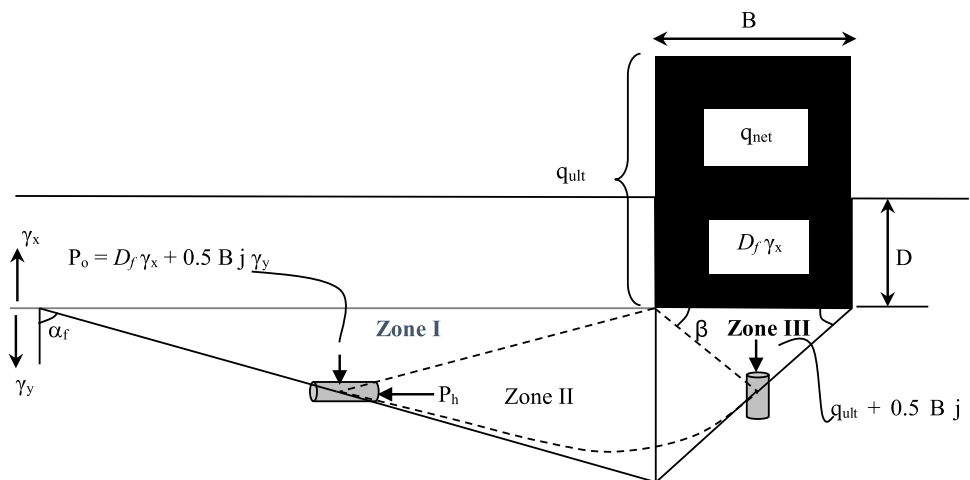


Fig. 2 Three zone Model–Mohr circle representation

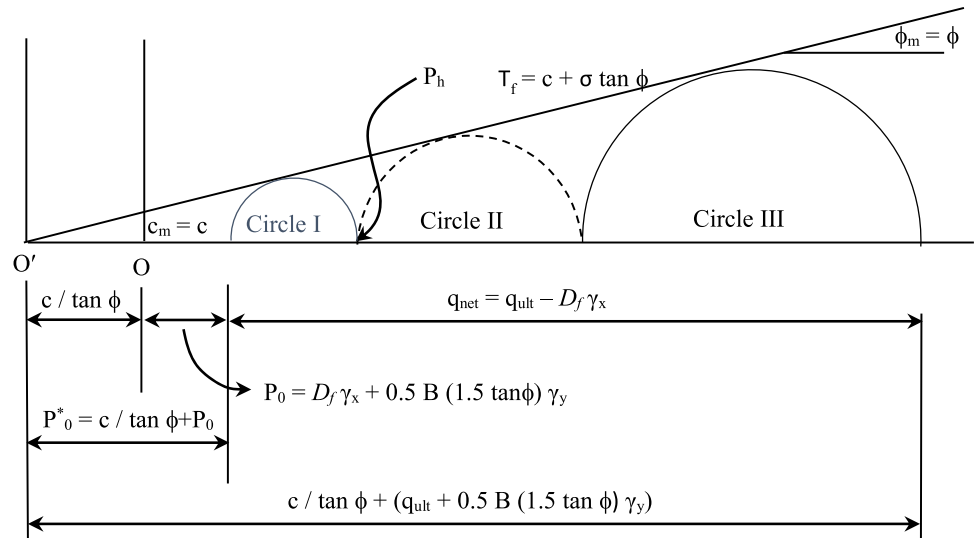
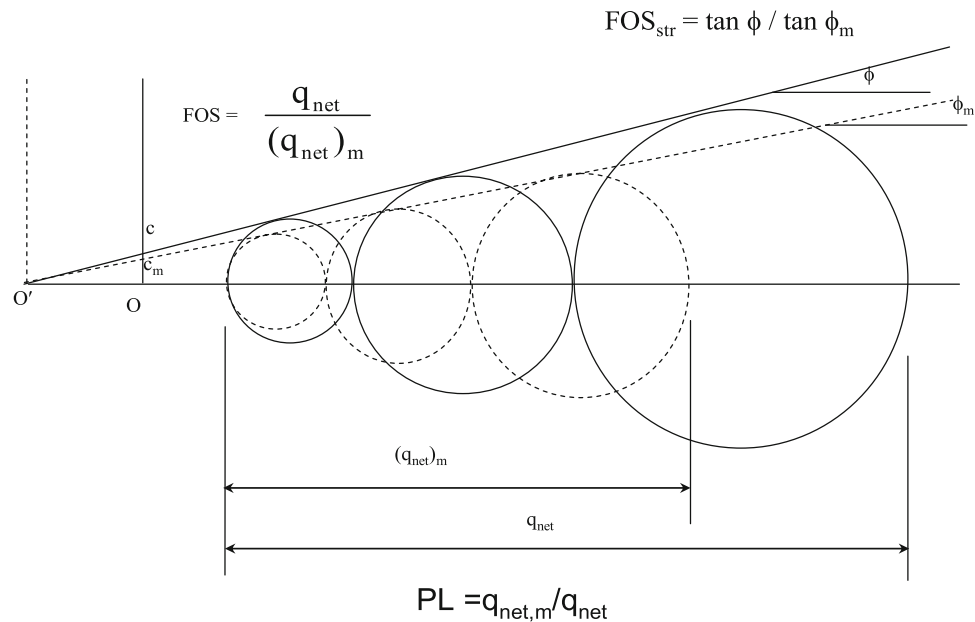


Fig. 3 FOS, FOS_{str} (based on shear strength) and PL (FOS reciprocal)



is the gross pressure at foundation base minus the overburden pressure due to base embedment, i.e., $D_f \gamma_x$.

$$q_{net} = q_{ult} - D_f \gamma_x$$

Figures 1 and 2 characterize failure conditions, however, at some mobilized friction angle, ϕ_m , and mobilized cohesion, c_m , the distance noted as q_{net} , would instead be a net mobilized pressure, $q_{net,m}$. In fact, the traditionally defined factor of safety against (net) bearing capacity failure is the ratio $q_{net}/q_{net,m}$, while its reciprocal, $q_{net,m}/q_{net}$, is the pressure level, PL, both of which are pictured in Fig. 3. Alternatively, a factor of safety based on shear strength (as employed, for instance, in slope stability analysis) is the ratio of the slopes, $\tan\phi/\tan\phi_m$, also pictured in Fig. 3.

Single-layer soil structure

Load calculation

Based on the model depicted in Figs. 1 and 2, the resulting (net) ultimate bearing capacity becomes

$$q_{net} = P_o * (\tan^6 \alpha_f - 1), \tag{1}$$

where

$$\alpha_f = 45^\circ + f/2$$

$$P_o * = P_o + c / \tan \phi = D_f \gamma_x + 0.5 B (1.5 \tan \phi) \gamma_y + c / \tan \phi$$

while the equation for a given mobilized condition is

$$q_{net,m} = P_o * (\tan^6 \alpha_m - 1) \tag{2}$$

$$\alpha_m = 45^\circ + \phi_m/2$$

q_{net} and $q_{net,m}$ of Eqs. 1 and 2 are both expressed entirely in terms of a friction angle ϕ and or ϕ_m relative to O' with c (from $c/\tan \phi$) considered only as an effective stress (ES) component of P_o^* . Comparing Eq. 1 with the general (net) bearing capacity equation of Hansen, Vesic, and Meyerhof,

$$q_{net} = q_{ult} - D_f \gamma_x = 0.5 B \gamma_{yj} N_\gamma + D_f \gamma_x (N_q - 1) + c N_c, \tag{3}$$

where

$$N_\gamma = (N_q - 1)$$

$$N_c = (N_q - 1) / \tan \phi$$

$$q_{net} = D_f \gamma_x (N_q - 1) + 0.5 B \gamma_{yj} (N_q - 1) + c / \tan \phi (N_q - 1)$$

$$= [D_f \gamma_x + 0.5 B \gamma_{yj} + c / \tan \phi (N_q - 1)] (N_q - 1)$$

Since

$$P_o^* = D_f \gamma_x + 0.5 B (1.5 \tan \phi) \gamma_y + c / \tan \phi$$

this yields

$$q_{net} = P_o^* (N_q - 1)$$

Hansen, Vesic, and Meyerhof's N_q for the strip footing is given by

$$N_q = e^{(\pi \tan \phi)} [\tan^2(45 + \phi/2)]$$

By comparison, N_q for the proposed model is given, for a square or circular rigid foundation (with no additional shape correction), with negligible depth correction and using standard triaxial test's stress-strain and strength response, as

$$N_q = \tan^6(45 + \phi/2)$$

Hansen, Vesic, and Meyerhof's equation and the proposed model equations differ in terms of j , where

$$j = 1.5 \tan \phi \text{ for Hansen and the proposed model}$$

$$j = 1.5 \tan \phi \text{ for Meyerhof}$$

$$j = 2 \tan \phi (N_q + 1) / (N_q - 1) \text{ for Vesic}$$

The proposed model assumes the same stress level (SL) in all three zones for a mobilized condition, though the strain might not be the same in all three zones at this SL. The effect of soil compressibility on the stress state can be accounted via changing the secant friction angle as a function of the corresponding current effective confining pressure ($\sigma'_{3,m}$) in each of the three zones, see Fig. 4. While Fig. 4 illustrates the angles at failure, it can be shown that the corresponding value of mobilized friction

angle in terms of the peak value at the same confining pressure at the specified stress level (SL) is

$$\sin \phi_m = SL A / (SL A + 2) \tag{4}$$

$$A = \tan^2(45 + \phi/2) - 1 = 2 \sin \phi / (1 - \sin \phi)$$

Since the model considers a square or circular foundation, the stress state in zones II and III represent conditions in any radial direction (from vertical centerline of the footing). The stress and strain that occurs in zone III of Fig. 1 can be thought of as what occurs in the upper cone of a standard triaxial test (with due consideration for the changing confining pressure of zone III). Since there is full friction between the base and underlying soil of the foundation, this is equivalent to the standard triaxial test with friction between the soil and cap or base at the ends of the soil specimen. Elfass et al. [2] provides more details on the load calculations.

Settlement Calculation

Foundation settlement, ρ , is directly related to the peak vertical or major principal strain, ϵ , of zone III of the Schmertmann et al. [3] strain triangle over depth $2B$ (for the square and circular foundation). The strain, ϵ , is the current deviatoric stress of zone III ($\sigma_d = \Delta \sigma'_1 - \Delta \sigma'_3$) divided by the secant Young's modulus, E , corresponding to σ'_3 of zone III. Picture this as a point on a triaxial test stress-strain curve at that confining pressure (σ'_3). As $q_{net,m}$ increases, so does σ'_3 of zone III. As if the point of concern for zone III jumps from one triaxial test stress-strain curve to another.

Settlement, ρ , at any $q_{net,m}$ is equal to the area of the strain triangle or $\epsilon(B)$. (The area is the same whether ϵ is taken to occur at $0.5B$ or $0.5jB$.) One should note that σ_{dm} of zone III from the model increases from 0.5 to 0.75 of $q_{net,m}$ which corresponds quite well with Schmertmann's q_{Iz} (where $q = q_{net,m}$). The characterization of the triaxial test deviatoric axial stress-strain curve at constant confining pressure as presented by Ashour and Norris [4] is given in terms of SL (σ_{dm}/σ_{df}) as

$$\epsilon = SL \frac{e^{3.707SL} \epsilon_{50}}{\lambda}, \tag{5}$$

where ϵ_{50} is the strain at SL = 0.5 and λ is a function of triaxial test stress level, SL, i.e.,

$$\lambda = 3.19 \text{ for } SL < 0.5 \tag{6a}$$

$$\lambda = -7.1219 SL^2 + 7.0592 SL + 1.4403 \text{ for } SL > 0.5 \tag{6b}$$

Note that the triaxial test σ_{df} at constant confining pressure, σ'_3 , is

Fig. 4 Change in the secant friction angle from one zone to another

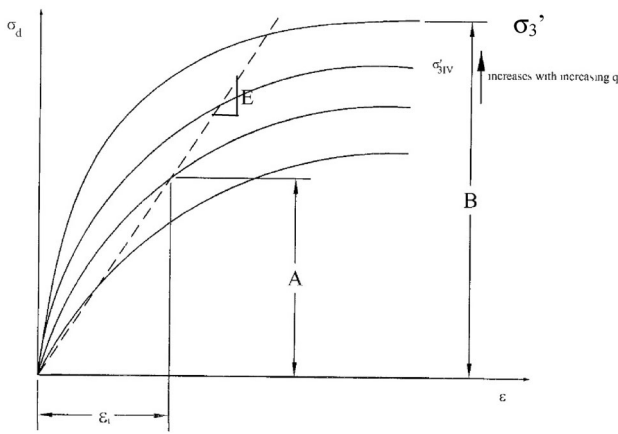
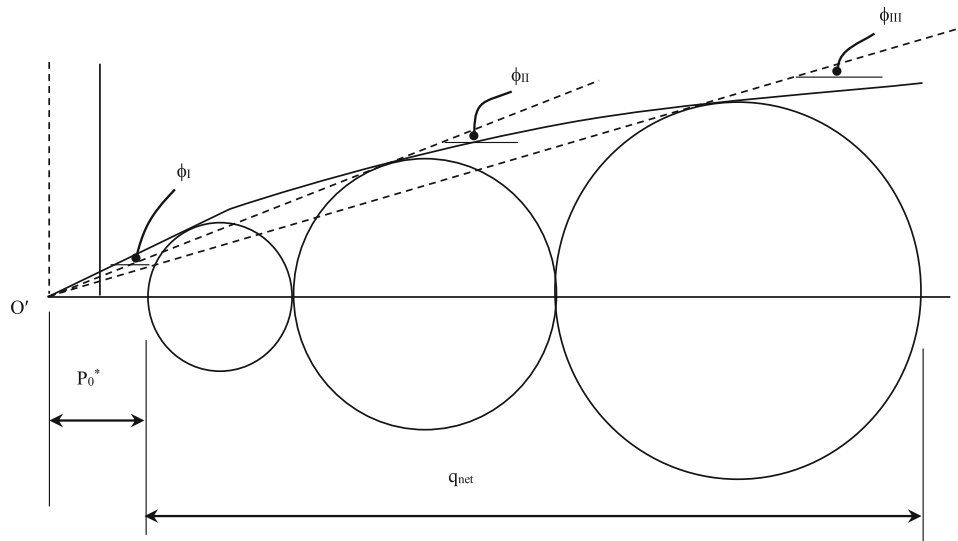


Fig. 5 Triaxial tests at different constant confining pressures

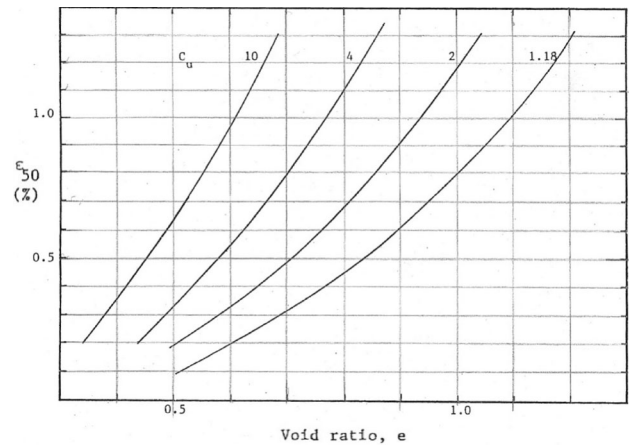


Fig. 7 $\epsilon_{50,ref}$ (%) at $\sigma_{3,ref}' = 0.87$ ksf as a function of void ratio (e) and uniformity coefficient (C_u)

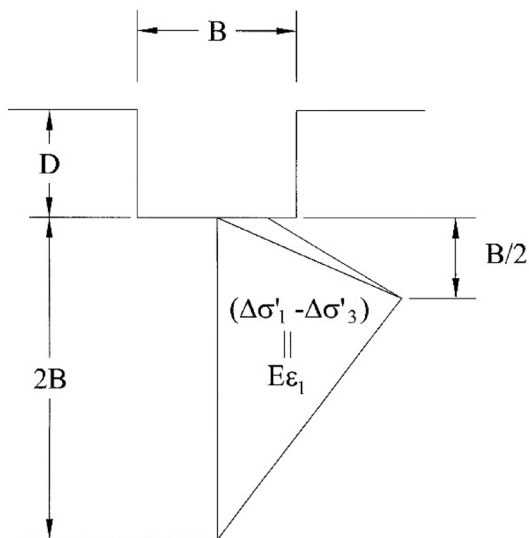


Fig. 6 Strain at 0.5 B of the Schmertmann triangle

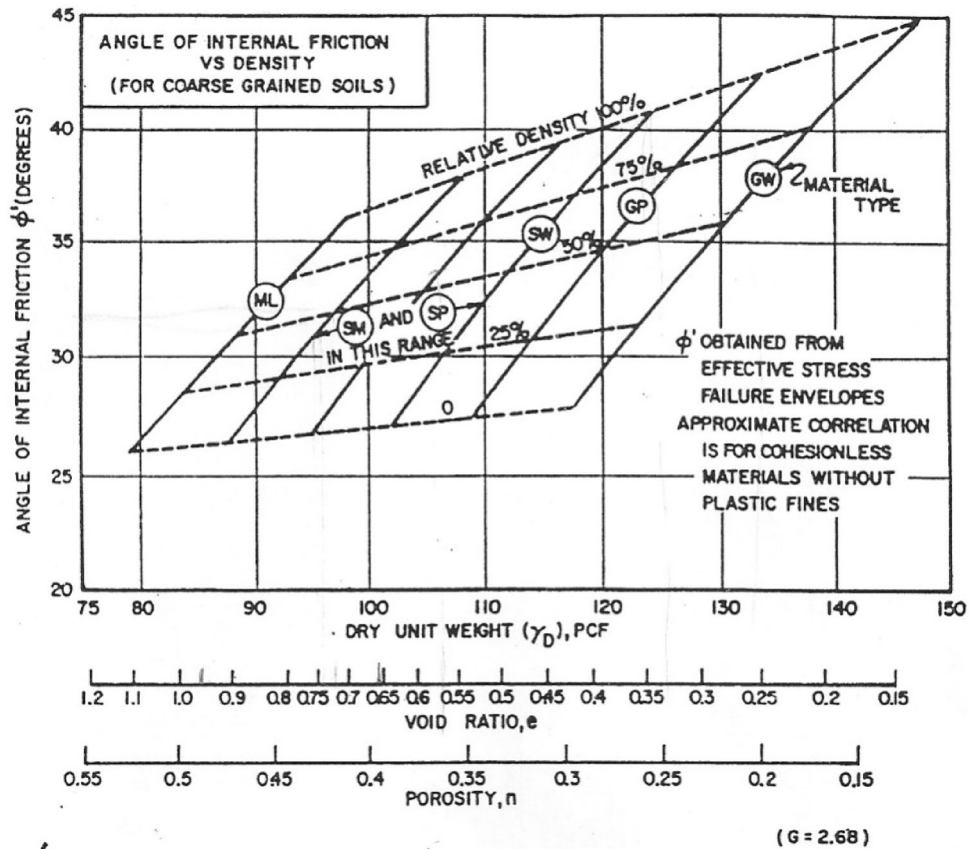
$$\sigma_{df} = A\sigma_3' \tag{7}$$

A is presented in Eq. (4). Figures 5 and 6 illustrate the consideration of SL, as if from the triaxial test stress–strain curve relative to the current confining pressure of zone III. Note that ϵ_{50} of zone III will vary with confining pressure $\sigma_{3,m,III}'$ as given by

$$\epsilon_{50,III} = \epsilon_{50,ref} (\sigma_{3,m,III}' / \sigma_{3,ref}')^n; \quad n = 0.2-0.3 \tag{8}$$

While $\epsilon_{50,ref}$ is best obtained from the triaxial test stress–strain curve conducted at constant confining pressure, $\sigma_{3,ref}'$, obtaining an undisturbed sample from below where the foundation is to be located is not always achievable. In such cases, $\epsilon_{50,ref}$ may be estimated from Fig. 7 corresponding to a reference pressure of 0.425 kg/cm² (~ 42.5 kPa) or 0.87 ksf. Note that Eq. 8 takes account of the effect of the soil’s compressibility on stress–strain behavior. On the other hand, if triaxial tests on undisturbed

Fig. 8 Chart for evaluating ϕ_{ref} at an assumed $\sigma_{3' ref}$ of 1 tsf taken from DM 7.1 [5], page 149



samples are not available, the friction angle, ϕ , can be estimated based on Fig. 8 taken from DM 7.1 [5].

Multi-layer soil structure

Soil structures often consist of more than one type of soil. In fact, even when a single type of soil is present, the variability in soil properties is often handled by subdividing the soil structure into multiple layers, to account for the variation in properties (e.g., dense sand, loose sand). Hence, there is the additional challenge of estimating the ultimate bearing capacity of shallow foundations resting on layered soil structures.

Load calculation

In case of multi-layer soil structure, the zone of the soil structure contributing to the estimated load is assumed to extend up to a depth of B below the foundation level. In the beginning, each layer of the soil structure within the influence zone is treated separately, repeating the same calculation procedure outlined for a single-layer soil structure. Then to combine the layered soil structure effect,

the load, P, resulting from a number of influential layers, n, within a depth of B is expressed as

$$P = \frac{1}{B} (P_1 H_1 + P_2 H_2 + \dots + P_n H_n), \tag{9}$$

where H_i (H_1, H_2, \dots, H_n) are the layers' thicknesses.

Settlement calculation

To estimate the settlement response corresponding to the estimated load, the zone of influence is presented in Schmertmann et al. [3] strain triangle, where the foundation settlement is directly related to the peak vertical or major principal strain, ϵ , of zone III over depth 2B (for the square and circular foundation) of the strain triangle. Each layer of the soil structure within the influence zone is treated separately in the beginning, repeating the same calculation procedure outlined for a single-layer soil structure. Then to combine the layered soil structure effect, the area of the strain triangle for each soil layer is normalized by the total area of the triangle. The foundation settlement, ρ , is then calculated as follows:

$$\rho = \frac{1}{Area_{(T)}} (Area_1 \rho_1 + Area_2 \rho_2 + \dots + Area_n \rho_n), \tag{10}$$

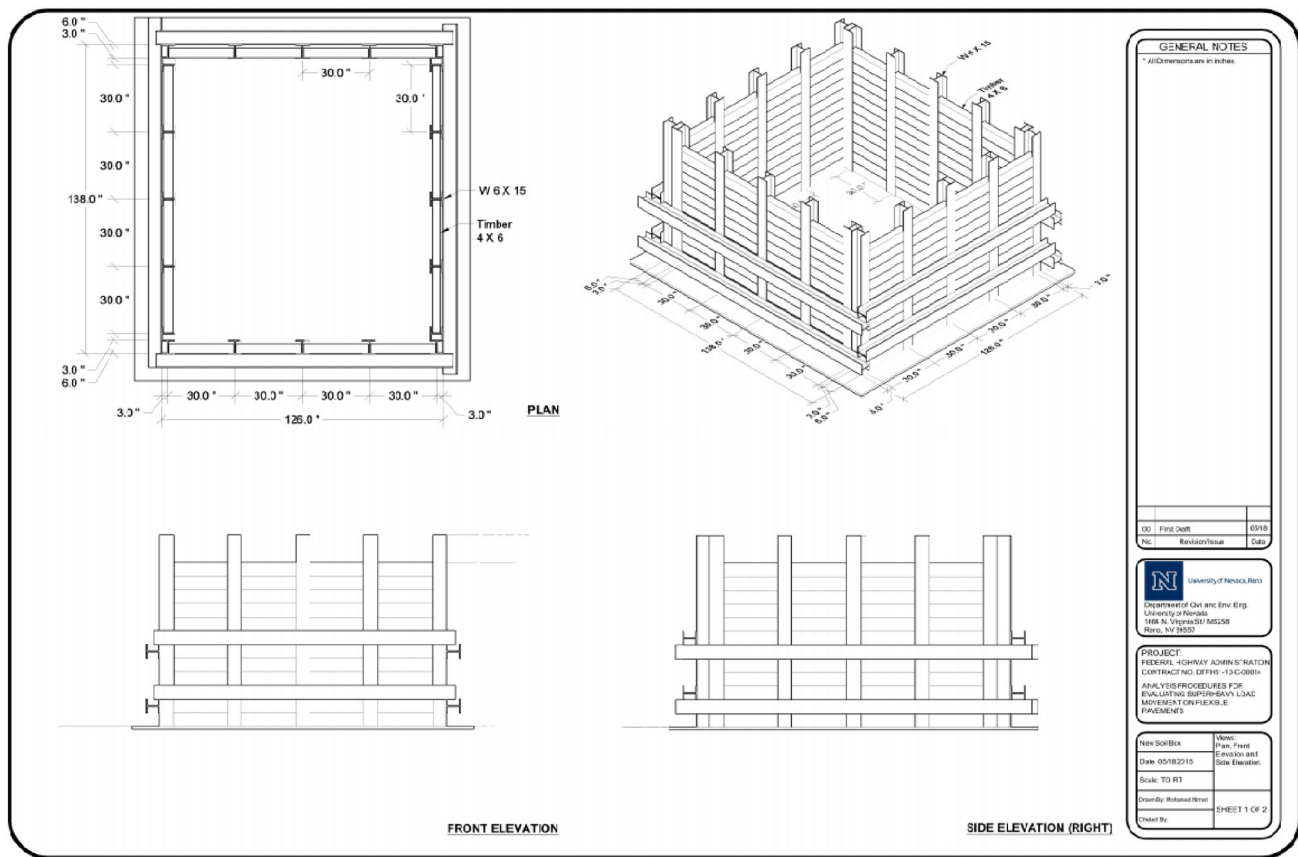


Fig. 9 Illustration, plan, front elevation, side elevation, and isometric view of UNR large-scale box

where $Area_i$ ($Area_1, Area_2, \dots, Area_n$) are Area(s) of the strain triangle corresponding to the layer thickness H_i . $Area_{(T)}$ is total Area of strain triangle.

Validation of proposed model

Two full-scale experiments were recently performed at the University of Nevada, Reno (UNR), as part of UNR’s large-scale pavement/soil experimental program. The experiments modeled single-layer and multi-layer soil structure utilizing a large soil box 10 ft. (3.048 m) × 10 ft. (3.048 m) × 7 ft. (2.134 m). The load–settlement responses up to bearing capacity failure have been obtained for both experiments. However, material characterization is yet to be completed, and prediction of the load–settlement response using the proposed model is yet to be presented.

A few of the well-documented full-scale field and lab tests were used to calibrate or validate the proposed model. Three sets of tests were used to calibrate or validate the proposed model, FHWA/ASCE footing tests undertaken at the Texas A&M University field test site [6], the lab tests performed on circular footings at the Suez Canal University, [7] and the lab tests performed at the University of Strathclyde [8].

UNR large-scale experiments

Two full-scale plate load experiments were performed at the large-scale pavement/soil testing facility at UNR, utilizing a large pavement/soil box 10 ft. (3.048 m) × 10 ft. (3.048 m) × 7 ft. (2.134 m) height. An illustration of UNR large-scale box is presented in Fig. 9. These experiments are part of a larger pavement experimental program, aiming to verify multiple theoretical approaches. Two types of loading were applied in each experiment. The testing was initially dynamic with increasing amplitudes, up to about 10% of the anticipated bearing capacity load level. The soil structure was then allowed to recover for 30 min. Then, an increasing static load was applied up to failure, with a constant settlement rate of 0.4 in/min (10 mm/min). All loads were applied on the loading plate positioned directly at the top of the soil structure and at the center of the large-scale box. Table 1, provides a brief description of the two experiments and the loading protocol. The recorded load–settlement response for both UNR experiments are shown in Fig. 12.

Experiment No. 1 of UNR’s large scale consisted of a single-layer $c-\phi$ soil structure (soil₁), with a total thickness of 5.5 feet (1.676 m). Soil₁ is currently being tested at

Table 1 UNR large-scale box experiments, material properties, and loading protocol

Exp. no.	Soil description	Soil strength parameters consolidated drained (CD) triaxial test		Atterberg limits			Max. dry density	Max. wet density	Optimum moisture content	Loading protocol	Load plate diameter
		c	ϕ	LL	PL	PI					
1	Single type of soil ₁ with a thickness of 5.5 feet (1.676 m)	1.64 psi (11.3 kPa)	38.2°	43.0	22.8	20.2	125.5 pcf (19.7 kN/m ³)	140.3 pcf (22.0 kN/m ³)	11.8%	Apply increasing static load, with a constant loading Rate of 0.4 inch/min (10 mm/min) until failure	11.9 inch (300 mm) circular steel plate
2	Two types of soil 0.5 ft (0.152 m) of soil ₂ on top of 5.5 feet (1.676 m) of soil ₁ Total thickness is 6.0 feet (1.829 m)	0.00 psi ^a	42.0° ^a	N/A	N/A	0	138.2 pcf (21.7 kN/m ³)	149.7 pcf (23.5 kN/m ³)	8.3%		

^a The c - ϕ values of soil₁ (CAB) were estimated using Fig. 8 taken from DM 7.1 [5], page 149

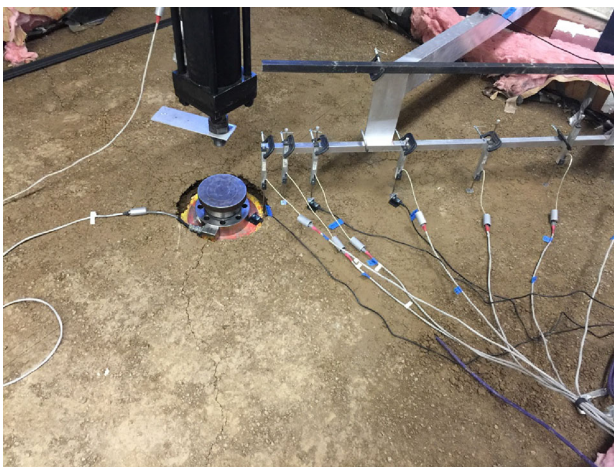


Fig. 10 Completed UNR’s large-scale Experiment No. 1



Fig. 11 Completed UNR’s large-scale Experiment No. 2

Table 2 Texas A&M field tests, footing dimensions, and material properties

Footing no.	Length, L (m)	Width, B (m)	Embedment depth, D (m)	Avg. $N_{1,60}$ D to $D + B$	ϕ° from PH&T ^a	ϕ° from triaxial tests
1	0.991	0.991	0.711	26.0	34.8	34.0
2	1.505	1.492	0.762	23.6	33.2	
3	2.489	2.496	0.762	22.8	32.8	
4	3.004	3.004	0.762	23.5	33.2	
5	3.023	3.016	0.889	22.5	32.6	
Average					33.3	

^a Friction angles for the sand beneath each foundation were estimated for model use from the nearest borehole’s SPT $N_{1,60}$ values using a modified Peck, Hanson, and Thornburn chart (with additional curves for fines and PI) from Florida DOT [9]

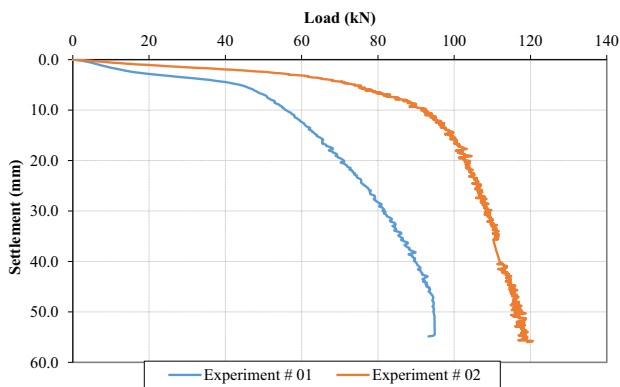


Fig. 12 Recorded load–settlement response of UNR large-scale experiments

UNR geotechnical laboratories and the results of Atterberg limits test, consolidated drained (CD) triaxial tests and proctor test are presented in Table 1. In Experiment No. 2, a two-layer soil structure was used, where two types of soil were used. 6 inch (0.152 m) of soil₂ on top of 5.5 feet (1.676 m) of soil₁, with a total thickness of 6.0 feet (1.829 m). Soil₂, a type 2 class B crushed aggregate base (CAB), was used in large-scale box Experiment No. 2. The CAB material was selected following the Nevada department of transportation (NDOT) materials’ specification for dense graded CAB. Soil₂ properties are also presented in Table 1. Figures 10 and 11 show the completed large-scale experiments.

Texas A&M tests

Five well-documented foundation tests from the Texas A&M field site are considered. Details of the tests are reported in an ASCE Geotechnical Special Publication No. 41 [6]. Sand with approximately 16% nonplastic fines (SM) and relative density, D_r , of 55% is found at the site. Table 2 summarizes the footing dimensions, the $N_{1,60}$ blow count values and chart assessed friction angles determined for the sand within the depth D_f to $D_f + B$ below the base of each footing and, separately, reported triaxial test results. The ϵ_{50+ref} values were

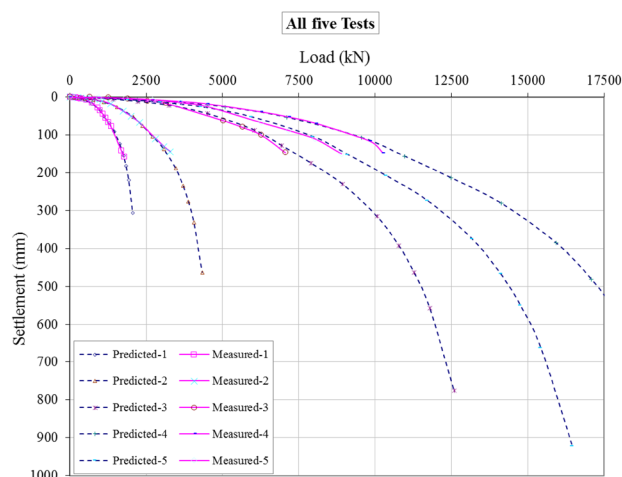


Fig. 13 Model predicted versus recorded load–settlement response of the five Texas A&M tests

established from the triaxial test stress–strain data. A value of 0.6% at 870 psf was used.

Model-predicted load–settlement behavior is plotted versus the recorded response for all five footings in Fig. 13. One should consider such comparison as a calibration of the model because the cohesion value of the soil was varied for each case to give the best match of the predicted to the recorded response.

Suez Canal University lab tests

Five lab tests from the Suez Canal University are considered. Details of the tests are reported in Housing and Building National Research Center (HBRC) Journal [7]. Table 3 summarizes the footing dimensions and material properties. Model-predicted load–settlement behavior is overlaid on the recorded response for two of the footings in Figs. 14 and 15. A good agreement between measured and predicted load–settlement response is observed. This observation indicates that the model predicts the load–settlement response with reasonable accuracy for the reported test conditions and material properties.

Table 3 Suez Canal University lab tests, material properties

Element	Soil type	Model	c (kPa)	ϕ	ψ	γ (kN/m ³)	E_s (kN/m ²)	ν
Upper layer (drained)	Medium to loose sand (series 1)	Mohr column	1	35	5	19	20,000	0.3
	Very dense sand (series 2)	Mohr column		45	12	22	50,000	0.29
Lower layer (undrained)	Soft clay	Mohr column	21	0	0	20	4000	0.5
Footing	Steel	Elastic	–	–	–	–	2E + 08	0.3

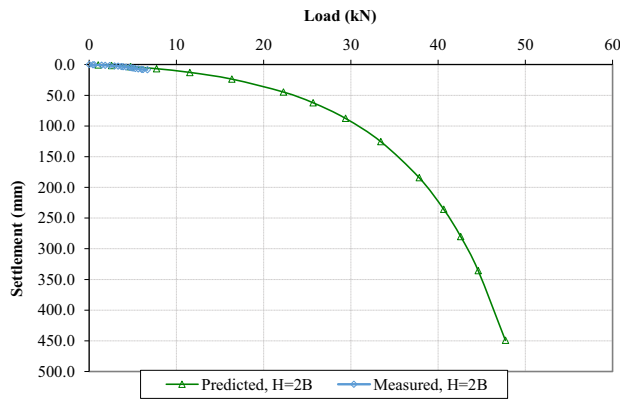


Fig. 14 Model predicted versus recorded load–settlement response of Suez Canal University lab tests

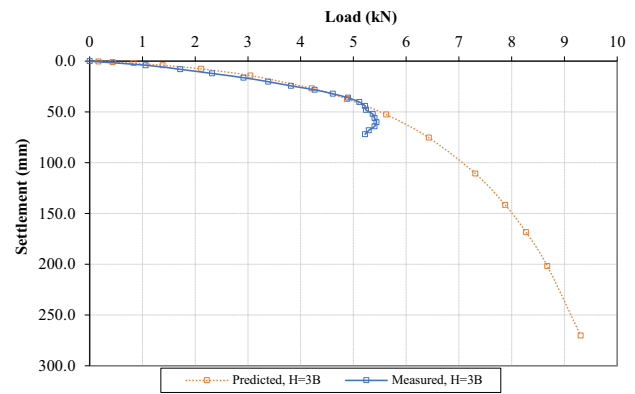


Fig. 16 Model predicted versus recorded load–settlement response of University of Strathclyde experiments

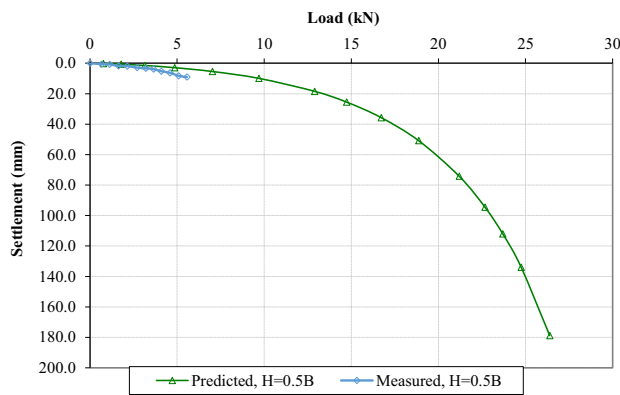


Fig. 15 Model predicted versus recorded load–settlement response of Suez Canal University lab tests

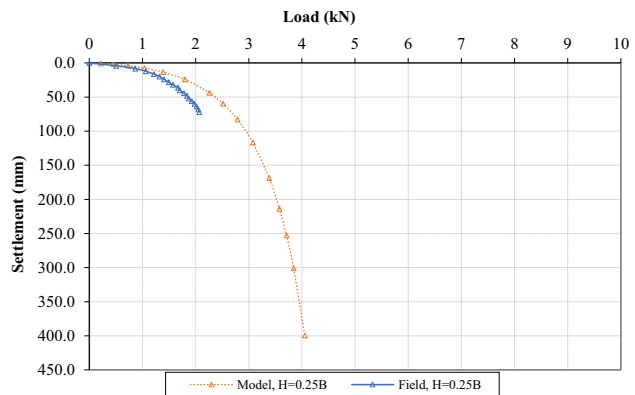


Fig. 17 Model predicted versus recorded load–settlement response of University of Strathclyde experiments

Table 4 University of Strathclyde experiments, properties of the fill material (Leighton Buzzard sand)

Property	Values
Mineral composition	Mainly quartz
Specific gravity	2.65
Particle size range	0.3–2.0 mm
Uniformly coefficient, d_{60}/d_{10}	1.22
Mean diameter, d_{50}	0.85 mm
Porosity limits	34.0% (min.) to 44.5% (max.)

University of Strathclyde experiments

Several experiments from the University of Strathclyde experimental program are presented here. Details of the testing are reported by Kenny and Andrawes [8]. A strip footing 0.12-m wide, placed in a tank (2.0 m length \times 0.3 m width \times 1.4 m height), was employed in

all tests. A soft clay subgrade (with undrained ϕ_u of 0 and an average c_u of 10.6 kN/m²) overlain by uniformly graded coarse Leighton Buzzard sand (dense) was used under the footing. Properties of the Leighton Buzzard sand are presented in Table 4.

Model-predicted load–settlement behavior is shown side by side with the recorded response for two of the footings in Figs. 16 and 17. Comparing the measured and predicted load–settlement response, the model again predicts the load–settlement response reasonably well for the reported testing conditions and material properties, given that the clay is not a granular material as the model assumes.

Conclusions

A numerical model for shallow foundation load–settlement response up to bearing capacity failure has been presented and calibrated/verified against both bearing capacity and load–settlement response reported in the literature. It is

easily programmed in a spreadsheet and can be used for design to assess true bearing capacity or more importantly to develop a curve of predicted load–settlement response, which can be used to define any desired failure criteria. It can likewise be used to develop specific analysis charts or to undertake a sensitivity study of input parameter effects on response. A similar model for undrained soil conditions (i.e., strength $S_u = c$) based on the same principles is also possible. The experiments performed at UNR's large-scale pavement/soil testing facility show very interesting results, where the testing is continued to ultimate bearing capacity. These experiments will help further verify/calibrate the model at higher load levels once material characterization is complete and fully reported.

References

1. ASCE (1993) Bearing capacity of soils technical engineering and design guides as adopted from the US Army Corps of engineers, No. 7. ASCE Press, New York
2. Elfass SA, Norris GM, Vimalaraj P (2007) A simple bearing capacity equation. GeoDenver 2007, ASCE, new peaks in geotechnics. In: Advances in shallow foundations, GSP, vol 171, pp 1–10
3. Schmertmann JH et al (1978) Improved strain influence factor diagrams. J Geotech Eng Div ASCE 104(GT8):1131–1135
4. Ashour M, Norris GM (1999) Liquefaction and undrained response evaluation of sands from drained formulation. J Geotech Geoenviron Eng 125(8):649–658
5. U.S. Navy (1986, updated from 1982) NAVFAC DM 7.1 Design manual: soil mechanics
6. Briaud RL, Gibbens RM (1994). Predicted and measured behavior of five spread footings on sand. Geotechnical Special Publication No. 41, ASCE Press
7. Ibrahim KMHI (2014) Bearing capacity of circular footing resting on granular soil overlying soft clay. HBRC Journal 12:71–77
8. Kenny MJ, Andrawes KZ (1997) The bearing capacity of footings on a sand layer overlying soft clay. Geotechnique 47(2):339–345
9. Florida Department of Transportation (2004) Soils and foundation handbook